Quantum control of ultrafast magnetic field in H_3^{2+} molecules by tricircular polarized laser pulses

Qing-Yun Xu(徐清芸), Yong-Lin He(何永林), Zhi-Jie Yang(杨志杰), Zhi-Xian Lei(雷志仙), Shu-Juan Yan(闫淑娟), Xue-Shen Liu(刘学深), and Jing Guo(郭静)[†]

Institute of Atomic and Molecular Physics, Jilin University, Changchun 130012, *China*

(Received 11 June 2022; revised manuscript received 2 September 2022; accepted manuscript online 9 September 2022)

We present a scheme to control the generated ultrafast magnetic field in H_3^{2+} molecules using multi-frequency tricircular pulses composed of co- and counter-rotating bicircular pulses. Simulations show that the field amplitude and the wavelength are two significant factors for magnetic field generation by tricircular pulses. Specifically, the strength of the magnetic field is linearly related to the field amplitude at $\lambda_0 = 50$ nm, while at $\lambda_0 = 70$ nm, the strength first increases and then decreases with the amplitude, this can be attributed to the resonance between the ground and excited states. Moreover, the phase and helicity of bicircular pulses are shown to have important effects on the magnetic field. The dependence of the magnetic field on the phase arises from the interference effect between multiple ionization pathways. These findings illustrate a guiding principle for controlling the magnetic field in molecular systems for future research in ultrafast magneto-optics.

Keywords: magnetic field, tricircular pulses, field amplitude, phase, helicity

PACS: 32.80.Rm, 32.80.–t, 42.25.Kb, 42.65.Re **DOI:** 10.1088/1674-1056/ac90b6

1. Introduction

With the rapid advance of attosecond physics,[1–3] it has become important to explore the electron dynamics within molecular systems. By using attosecond pulses, electron dynamics on the natural attosecond time scale can be visualized and controlled.[4–8] In particular, the development of attosecond technology has extended from linearly polarized to circularly polarized (CP) pulses. Since CP pulses have a two-dimensional polarization plane and their ellipticity can provide additional freedom for electron motion, they are now proposed as a useful tool for studying attosecond electron dynamics.[9–11]

In recent years the magnetic phenomena generated by laser fields have attracted extensive attention due to their potential applications in many fields, such as magnetic data recording and femtosecond opto-magnetism.[12] Researchers have found that few-femtosecond CP and π laser pulses can be applied to induce electronic ring currents and associated induced magnetic fields in oriented molecules.[13–15] The generated magnetic fields can be much larger than those obtained with traditional static fields.[16,17] Recently, based on an attosecond time scale, a new attosecond magnetization has been realized.[18–25] Much effort has been devoted to investigating the dependence of ultrafast magnetic field generation from coherent electronic currents in H_2^+ on the laser parameters and molecular alignment.[19,23,25] Moreover, the generation of ultrafast magnetic fields from the point of view of resonance excitation of H_3^{2+} molecules by monochrome CP laser pulses has also been explored.[26] Indeed, similar magnetic phenomena have also been demonstrated in recent studies. For example, applying structured light to coherent control in a semiconductor allows the structure from optical frequency light to be transferred to currents and THz radiation and their accompanying magnetic fields.[27] Notably, coherent control of electron dynamics in strong fields includes not only coherent resonance between electronic states but also coherence induced by quantum interference between two or more laser fields. Currently, multiple color CP laser pulses have been used to theoretically explore these highly nonlinear optical phenomena.[28] However, research about magnetic field generation under multiple color CP laser pulses is scarce, and this field is worthy of further exploration.

In previous work we studied magnetic field generation of H_3^{2+} molecules induced by monochrome CP laser pulses.[26] This work further explores the induced magnetic fields under intense tricircular laser pulses by numerically solving the corresponding fixed nuclei time-dependent Schrödinger equation (TDSE). Results show that the generated magnetic field presents a linear relationship with the field amplitude of the bicircular pulses with a co-rotating component in tricircular laser pulses under the multi-photon ionization mechanism, which is different under the resonance excitation mechanism. In addition, the phase and helicity of the bicircular pulses also have important effects on the magnetic field due to interference between multiple ionization pathways.

[†]Corresponding author. E-mail: gjing@jlu.edu.cn

© 2023 Chinese Physical Society and IOP Publishing Ltd

2. Theoretical methods

The interaction between the laser field and H_3^{2+} is described by the two-dimensional TDSE

$$\mathrm{i}\frac{\partial\psi(\boldsymbol{r},t)}{\partial t}=\left[H_0(\boldsymbol{r})+H_{\rm int}(\boldsymbol{r},t)\right]\psi(\boldsymbol{r},t). \tag{1}$$

In this equation, the Hamiltonian with the field-free $H_0(\boldsymbol{r})=(p_x^2+p_y^2)/2+V_{\rm c}(\boldsymbol{r})$, where $(p_x^2+p_y^2)/2$ is the molecular kinetic term and the molecular Coulomb potential $V_{\rm c}(\boldsymbol{r})$ term can be written as

$$V_{\rm c}(\boldsymbol{r})=-\sum_{i=1}^{3}\frac{1}{\sqrt{(x-N_{ix})^2+(y-N_{iy})^2+\beta}}. \tag{2}$$

Figure 1 shows the molecular geometry of H_3^{2+}. The molecule is aligned along the x-axis; the rationality of such practice has been demonstrated in previous research.[26,29] The nuclear coordinates N_{ix} and N_{iy} of H_3^{2+} are fixed, $N_{1x}=0$, $N_{2x}=-R\sin(\theta/2)$, $N_{3x}=+R\sin(\theta/2)$, $N_{1y}=(2/3)R\cos(\theta/2)$, $N_{2y}=-(1/3)R\cos(\theta/2)$, and $N_{3y}=-(1/3)R\cos(\theta/2)$. $R=2$ is the distance between two protons and $\theta=60^\circ$ is the angle between two molecular bonds. A soft parameter $\beta=0.4$ a.u. is used to remove the Coulomb singularity and to meet the eigenenergy (-1.81 a.u.) of the ground A' state for H_3^{2+}.

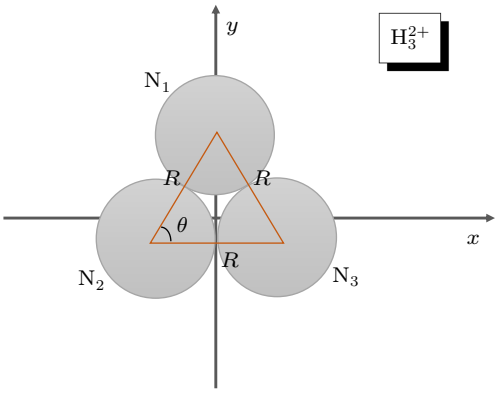


Fig. 1. Molecular geometry of H_3^{2+} with equilateral triangle geometry. N_i denotes the nucleus, where $i=1$, 2, and 3. R represents the molecular internuclear distance and $\theta=60^\circ$ is the bond angle between two molecular bonds.

The $H_{\rm int}=r\cdot E(t)$ is the field–molecule interaction. For tricircular laser pulses, $E(t)$ has the form

$$\boldsymbol{E}(t)=\boldsymbol{E}_1(t)+\boldsymbol{E}_2(t)+\boldsymbol{E}_3(t)=E_0 f(t)\begin{Bmatrix}\hat{e}_x\left[(1+\eta)\cos(\omega_1 t+\phi_{\omega_1})+\cos(\omega_2 t+\phi_{\omega_2})+\eta\cos(\omega_3 t+\phi_{\omega_3})\right]\\ \hat{e}_y\left[(1+\eta)\sin(\omega_1 t+\phi_{\omega_1})+\xi_1\sin(\omega_2 t+\phi_{\omega_2})+\eta\xi_2\sin(\omega_3+\phi_{\omega_3})\right]\end{Bmatrix}, \tag{3}$$

where η is the field amplitude of the $\boldsymbol{E}_1(t)$ and $\boldsymbol{E}_3(t)$ pulses. $\phi_{\omega_1}=\phi_{\omega_2}=\phi_{\omega_3}=0$ are the carrier envelope phases (CEPs) of the pulses $\boldsymbol{E}_1(t)$, $\boldsymbol{E}_2(t)$, and $\boldsymbol{E}_3(t)$. ξ_1 and ξ_2 present the helicities of the $\boldsymbol{E}_2(t)$ and $\boldsymbol{E}_3(t)$ pulses. In the length gauge, the field vector polarized in the molecular (x, y) plane, propagating along the perpendicular z-axis. From Eq. (3), we can obtain the bicircular laser pulses ($\omega_1+\omega_2$, $\xi_1=\pm1$, $\eta=0$) and tricircular laser pulses ($\omega_1+\omega_2+\omega_3$, $\xi_1=-1$, $\xi_2=+1$, $\eta\neq0$). A $\sin^2$ envelope $f(t)$ for a duration of 6τ ($1\tau=2\pi/\omega_0$), is used. E_0 is the amplitude of the field, corresponding to a laser intensity $I_0=c\varepsilon_0E_0^2$. Molecular TDSE in Eq. (1) is solved by a second-order accurate split-operator method with a time step of $\Delta t=0.05$ a.u. and the Fourier transform technique.[30,31] The initial wave packet is constructed by the imaginary time propagation method. The wave function at any time can be expressed as

$$\begin{aligned}&\psi(\boldsymbol{r},t+\Delta t)\\ &=\mathrm{e}^{-\mathrm{i}(p^2/4)\Delta t}\,\mathrm{e}^{(-\mathrm{i}V_{\rm c}(\boldsymbol{r})-\mathrm{i}H_{\rm int}(\boldsymbol{r},t))\Delta t}\,\mathrm{e}^{-\mathrm{i}(p^2/4)\Delta t}\psi(\boldsymbol{r},t)\\ &\quad+O(\Delta t)^3.\end{aligned} \tag{4}$$

The spatial coordinates are discretized by the grid points from -64 a.u. to 64 a.u., containing 512 grid points in both x- and y-directions, and the time step is $\Delta t=0.05$ a.u. Moreover, in order to prevent unphysical effects originating from the reflection of the wave packet from the boundary, the wave function is multiplied by a $\cos^{1/8}$ mask function at each time step. The domain of absorption $|x,y|$ ranges from 50 a.u. to 64 a.u.

The time-dependent electronic current density is defined by the quantum expression in the length gauge

$$\boldsymbol{j}(\boldsymbol{r},t)=-e\frac{\mathrm{i}}{2}\left[\psi(\boldsymbol{r},t)\nabla_{\boldsymbol{r}}\psi^*(\boldsymbol{r},t)-\psi^*(\boldsymbol{r},t)\nabla_{\boldsymbol{r}}\psi(\boldsymbol{r},t)\right], \tag{5}$$

where $\nabla_{\boldsymbol{r}}=\frac{\partial}{\partial x}\boldsymbol{i}+\frac{\partial}{\partial y}\boldsymbol{j}$ and $\psi(\boldsymbol{r},t)$ is the electron wave packet obtained from Eq. (1). Then, the corresponding time-dependent magnetic field $\boldsymbol{B}(\boldsymbol{r},t)$ can be obtained using the following classical Jefimenko equation:[32]

$$\begin{aligned}\boldsymbol{B}(\boldsymbol{r},t)\;=\;&-\mathrm{e}\frac{\mu_0}{4\pi}\int\left[\frac{\boldsymbol{j}(\boldsymbol{r}',t_{\rm r})}{|\boldsymbol{r}-\boldsymbol{r}'|^3}+\frac{1}{|\boldsymbol{r}-\boldsymbol{r}'|^2c}\frac{\partial\boldsymbol{j}(\boldsymbol{r}',t_{\rm r})}{\partial t}\right]\\ &\times(\boldsymbol{r}-\boldsymbol{r}')\,\mathrm{d}^3\boldsymbol{r}',\end{aligned} \tag{6}$$

where $t_{\rm r}=t-r/c$ is the retarded time and $\mu_0=4\pi\times10^7$ N·A^{-2} (6.692×10^{-4} a.u.). For the static induced magnetic field after the laser pulse, equation (6) reduces to the classical Biot–Savart law.

3. Results and discussion

We investigate the magnetic field generation of H_3^{2+} under tricircular laser fields. The form and schematic diagram of

the laser field can be seen in Eq. (3) and Fig. 2(a). The laser frequencies are $\omega_1 = \omega_0$, $\omega_2 = 2\omega_0$, and $\omega_3 = 4\omega_0$. Here, two wavelengths of $\lambda_0 = 50$ nm and 70 nm were considered, corresponding to $\omega_0 = 0.91$ a.u. $\left(\omega_1 < I_p, \omega_2 > I_p, \omega_3 > I_p\right)$ and 0.65 a.u. $\left(\omega_1 < I_p, \omega_2 < I_p, \omega_3 > I_p\right)$. Note that the ionization energy of the ground state A' of H_3^{2+} is $I_p(A') = 1.81$ a.u. The laser duration is $6\tau = 1.0$ fs for $\lambda_0 = 50$ nm and 1.4 fs for $\lambda_0 = 70$ nm. At $\lambda_0 = 50$ nm, ionization can occur by absorbing two ω_0 ($\omega_0 < I_p$), which corresponds to the two-photon ionization mechanism. At $\lambda_0 = 70$ nm, there is a resonance mechanism from ground state to first excited state. In the present calculations, the intensity of the tricircular laser pulses is fixed at $I_0 = 1 \times 10^{14}$ W/cm^2 ($E_0 = 0.0534$ a.u.). The ponderomotive energies $U_p = E_0^2/4\omega_0^2 = 8.6 \times 10^{-4}$ a.u. ($\omega_0 = 0.91$ a.u.) and 1.687×10^{-3} a.u. ($\omega_0 = 0.65$ a.u.) correspond to Keldysh parameters $\gamma = \sqrt{I_p/2U_p} = 32.4$ and $23.16 \gg 1$, implying a multiphoton process. Figure 2(b) shows the A' electronic ground state at equilibrium distance ($R = 2$ a.u.), which is obtained numerically from imaginary time propagation of the field-free TDSE in Eq. (1).

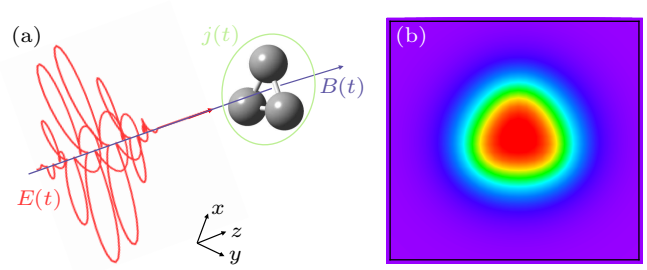


Fig. 2. (a) Illustration of the attosecond magnetic field $\boldsymbol{B}(t)$ (blue line, along the z-axis) for H_3^{2+} by an intense ultrashort tricircular laser pulse (red line). The green line represents the corresponding current $\boldsymbol{j}(t)$ in the molecular (x, y) plane. The magnetic field $\boldsymbol{B}(t)$ is perpendicular to the current. (b) Two-dimensional plots of the initial wave function density for the ground state A' of H_3^{2+} by numerically solving field-free TDSEs in Eq. (1).

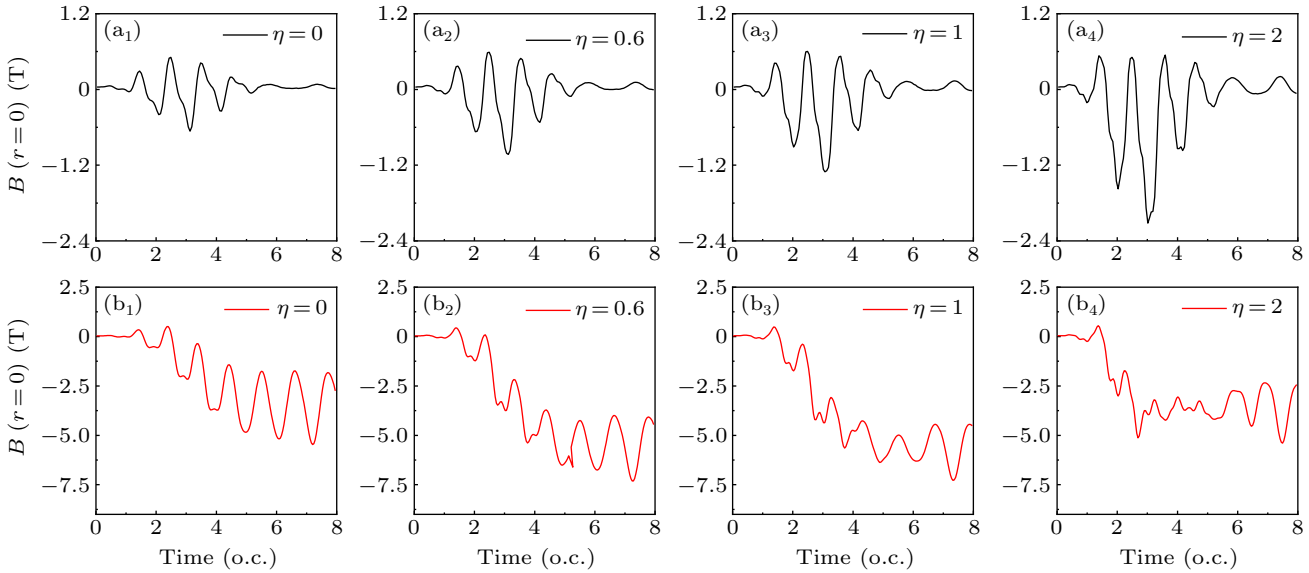


Fig. 3. The time-dependent magnetic field $\boldsymbol{B}(\boldsymbol{r} = 0, t)$ under different field amplitudes η of tricircular laser pulses with (a_1)–(a_4) $\lambda_0 = 50$ nm ($\omega_0 = 0.91$ a.u.) and (b_1)–(b_4) $\lambda_0 = 70$ nm ($\omega_0 = 0.65$ a.u.). The laser frequencies are $\omega_1 = \omega_0$, $\omega_2 = 2\omega_0$ and $\omega_3 = 4\omega_0$, the intensity is $I_0 = 1 \times 10^{14}$ W/cm^2 and the duration is 6τ (cycles).

Firstly, the effect of laser fields $E(t)$ with different field amplitudes (η) on the magnetic field was explored. As illustrated in Fig. 2(a), since the electronic currents are generated in the (x, y) plane, the induced magnetic fields are mainly localized along the z-axis, so we focus on the magnetic field $\boldsymbol{B}(\boldsymbol{r} = 0, t)$ at the center of the molecule. Figure 3 shows $\boldsymbol{B}(\boldsymbol{r} = 0, t)$ with different η for two wavelengths. As for the case of $\lambda_0 = 50$ nm (Figs. 3(a_1)–3(a_4)), we can find that $\boldsymbol{B}(\boldsymbol{r} = 0, t)$ is sensitive to η. At $\eta = 0$, 0.6, 1.0, and 2, $\boldsymbol{B}(\boldsymbol{r} = 0, t)$ are produced with maximum values of 0.661 T, 1.029 T, 1.304 T, and 2.119 T. These results indicate that an increase in η will give rise to a stronger magnetic field. It should be mentioned that at $\eta = 0$ the laser pulses were reduced to bicircular laser pulses (see Eq. (3)). From this, we compared the strengths of magnetic fields from bicircular and tricircular laser pulses. It is obvious that the generated magnetic fields are weaker by the former than by the latter, further confirming that tricircular laser pulses are more efficient at enhancing the magnetic field. Then, we studied the case of $\lambda_0 = 70$ nm (Figs. 3(b_1)–3(b_4)). When η is 0, 0.6, 1.0, and 2, the maximum value of $\boldsymbol{B}(\boldsymbol{r} = 0, t)$ is 5.469 T, 7.312 T, 7.278 T, and 5.392 T, respectively, indicating that the maximum magnetic field first increases and then decreases with the increase in η, which is different from the case of $\lambda_0 = 50$ nm.

In order to more intuitively see the effect of η on the magnetic field, the maximum values of the magnetic field $\boldsymbol{B}(\boldsymbol{r} = 0)$ with different η at two laser wavelengths (50 nm and 70 nm) are presented in Fig. 4. Here, the maximum values

are marked as $\boldsymbol{B}_{\rm m}$. It can be seen that $\boldsymbol{B}_{\rm m}$ and η show a linear relationship for $\lambda_0 = 50$ nm, while the relationship between $\boldsymbol{B}_{\rm m}$ and η at $\lambda_0 = 70$ nm is quite different. As η increases, $\boldsymbol{B}_{\rm m}$ also increases at first, and when η increases to 0.8, $\boldsymbol{B}_{\rm m}$ reaches a maximum value (7.387 T); then, when η continues to increase, the magnetic field begins to weaken. Additionally, the $\boldsymbol{B}_{\rm m}$ obtained at $\lambda_0 = 70$ nm is higher with a range of 3.27 T–4.8 T than that obtained at $\lambda_0 = 50$ nm. This is due to the different mechanisms by which multiphoton ionization and resonance excitation occurred at $\lambda_0 = 50$ nm and 70 nm, respectively. Resonant excitation is more conducive to the generation of magnetic fields.

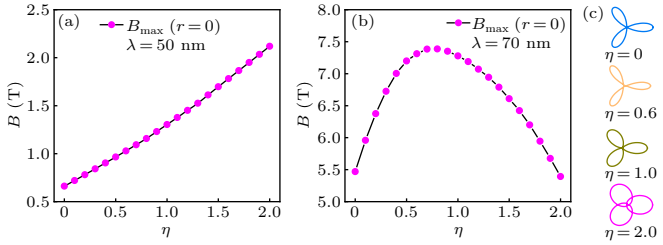


Fig. 4. Maximum values of the induced magnetic fields $\boldsymbol{B}(\boldsymbol{r}=0,t)$ with η by tricircular laser pulses with (a) $\omega_0 = 0.91$ a.u. ($\lambda_0 = 50$ nm) and (b) $\omega_0 = 0.65$ a.u. ($\lambda_0 = 70$ nm). (c) The parametric Lissajou curve of the driver fields with different η. The laser frequencies are $\omega_1 = \omega_0$, $\omega_2 = 2\omega_0$ and $\omega_3 = 4\omega_0$ and the intensity is $I_0 = 1\times10^{14}$ W/cm^2.

From Eq. (5), the electronic current $\boldsymbol{j}(\boldsymbol{r},t)$ is actually written as $j \sim \rho\nabla_r$. $\rho = |\psi(\boldsymbol{r},t)|^2$ is the continuum electron density. Therefore, the induced magnetic field $\boldsymbol{B}(\boldsymbol{r}=0)$ in Eq. (6) can be simplified to [note that the time-dependent term $(1/c)\partial\boldsymbol{j}(\boldsymbol{r},t)/\partial t$ in Eq. (6) is usually found to be negligible[23,25,33]]

$$\boldsymbol{B}(\boldsymbol{r},t) \sim \frac{\boldsymbol{j}}{\boldsymbol{r}^2} \sim \rho v/\boldsymbol{r}^2. \tag{7}$$

From Eq. (7), $\boldsymbol{B}(\boldsymbol{r}=0)$ is proportional to the electron probability density ρ and the electron velocity v, and inversely proportional to the square of current radius r.[25] Density ρ corresponds to the transition amplitude, which is determined by the transition dipole of the molecules and the electric field strength. Thus, the magnetic field is also proportional to the transition amplitudes. Next, we can adopt the ultrafast photoionization model[34,35] to understand the relationship between magnetic field on the field amplitude η in Fig. 4.

For the multiphoton ionization mechanism, the sensitivity of magnetic fields to η results from the interference caused by the multiphoton ionization channel during the modulation of two bicircular processes. The tricircular pulse $E(t)$ in Eq. (3) can be regarded as a combination of two bicircular pulses with counter-rotating and co-rotating components

$$\boldsymbol{E}(t) = \boldsymbol{E}^-(t) + \boldsymbol{E}^+(t), \tag{8}$$

where

$$\boldsymbol{E}^-(t) = E_0 f(t)\left\{\begin{array}{l}\hat{e}_x\left[\cos(\omega_1 t+\phi_{\omega_1})+\cos(\omega_2 t+\phi_{\omega_2})\right]\\ \hat{e}_y\left[\sin(\omega_1 t+\phi_{\omega_1})-\sin(\omega_2 t+\phi_{\omega_2})\right]\end{array}\right\},$$

$$\boldsymbol{E}^+(t) = \eta E_0 f(t)\left\{\begin{array}{l}\hat{e}_x\left[\cos(\omega_1 t+\phi_{\omega_1})+\cos(\omega_3 t+\phi_{\omega_3})\right]\\ \hat{e}_y\left[\sin(\omega_1 t+\phi_{\omega_1})+\sin(\omega_3 t+\phi_{\omega_3})\right]\end{array}\right\}.$$

Therefore, at $\lambda_0 = \lambda_1 = 50$ nm and $\lambda_2 = \lambda_1/2$ with a bicircular counter-rotating laser pulse $\boldsymbol{E}^-(t)$, the total transition probability is the square of the two amplitudes with an interference term of the cross products of the one-ω_2 and two-ω_1 photon ionization amplitudes; then, the total transition probability can be written as (for details see part 1 of the supporting information (SI))

$$\mathcal{F}^{(-)}_{2\omega_1+\omega_2} = |A_{2\omega_1}|^2 + |A_{\omega_2}|^2 + A^{(2\omega_1+\omega_2)}_{2\omega_1+\omega_2}. \tag{9}$$

The interference terms $A^{(2\omega_1+\omega_2)}_{2\omega_1+\omega_2}$ can be simply written as

$$\begin{aligned} A^{(2\omega_1+\omega_2)}_{2\omega_1+\omega_2} &\propto A^*_{2\omega_1}\cdot A_{\omega_2} + A^*_{\omega_2}\cdot A_{2\omega_1} \\ &= 2\sigma^{(1)}\sigma^{(2)}E_0(\omega_1)^2 E_0(\omega_2)\cos(\Delta\phi_1), \end{aligned} \tag{10}$$

where $\sigma^{(2)}$ and $\sigma^{(1)}$ are transition amplitudes of the one-ω_2 and two-$\omega_1+\omega_1$ photons and $\Delta\phi_1 = 2\phi_{\omega_1} - \phi_{\omega_2}$ is the phase difference.

Similarly, for a bicircular co-rotating laser pulse $\boldsymbol{E}^+(t)$, it is composed of simultaneous two-$\omega_1+\omega_1$ photons and one-$\omega_3 = 4\omega_1$ photons. The interference terms can be simply written as

$$\begin{aligned} A^{(2\omega_1+\omega_3)}_{2\omega_1+\omega_3} &\propto A^*_{2\omega_1}\cdot A_{\omega_3} + A^*_{\omega_3}\cdot A_{2\omega_1} \\ &= 2\sigma^{(1)}\sigma^{(3)}\eta^2 E_0(\omega_1)^2\,\eta E_0(\omega_3)\cos(\Delta\phi_2), \end{aligned} \tag{11}$$

where the relative phase difference $\Delta\phi_2 = \phi_{\omega_3} - 2\phi_{\omega_1} = 0$.

Based on the above, the total transition probability under a tricircular pulse in Eq. (3) ($E(t) = E^-(t) + E^+(t)$) is the sum of the square of the two amplitudes with their interference term

$$\mathcal{F}^{(-,+)} = \left|\mathcal{F}^{(-)}_{2\omega_1+\omega_2}\right|^2 + \left|\mathcal{F}^{(+)}_{2\omega_1+\omega_3}\right|^2 + \mathcal{F}^{(-,+)}_{2\omega_1+\omega_2,2\omega_1+\omega_3}, \tag{12}$$

where $\mathcal{F}^{(-,+)}_{2\omega_1+\omega_2,2\omega_1+\omega_3}$ is the simultaneous interference term, which can be expressed as

$$\begin{aligned} \mathcal{F}^{(-,+)}_{(2\omega_1+\omega_2,2\omega_1+\omega_3)} &\propto \mathcal{F}^{(-)*}_{2\omega_1+\omega_2}\cdot\mathcal{F}^{(+)}_{2\omega_1+\omega_3} + \mathcal{F}^{(+)*}_{2\omega_1+\omega_3}\cdot\mathcal{F}^{(-)}_{2\omega_1+\omega_2} \\ &= 8\sigma^{(1)}\sigma^{(2)}\sigma^{(1)}\sigma^{(3)}\eta^3 E_0(\omega_1)^2 E_0(\omega_2) \\ &\quad\times E_0(\omega_1)^2 E_0(\omega_3)\cos(\Delta\phi_3), \end{aligned} \tag{13}$$

where $\mathcal{F}^{(-)}_{2\omega_1+\omega_2}$ and $\mathcal{F}^{(+)}_{2\omega_1+\omega_3}$ are transition amplitudes of ionization from $E^-(t)$ and $E^+(t)$ bicircular pulses, and the relative phase is $\Delta\phi_3 = \phi_{\omega_2} - \phi_{\omega_3} = 0$. More details can be found in part 1 of the SI.

It can be seen from Eq. (13) that the interference term is proportional to η. As η increases, the interference term increases, thus the total transition probability in Eq. (13) is increased. Then, according to $\boldsymbol{B} \sim \rho v/\boldsymbol{r}^2$, we can see that the

magnetic fields increase with increasing transition probability, which can explain why the generated magnetic field becomes stronger as η increases in Fig. 4(a). However, for photon ionization of excited electronic states with intermediate resonances, the ionization probability can be written as[33,36]

$$W^{\mathrm{re}} \propto \langle \psi_{\mathrm{c}} | \boldsymbol{r}\cdot\boldsymbol{E} | \psi_{E'} \rangle \langle \psi_{E'} | \boldsymbol{r}\cdot\boldsymbol{E} | \psi_0 \rangle \sim W^{\mathrm{ie}} W^{\mathrm{ic}}, \quad (14)$$

where W^{ie} and W^{ic} are the transition dipole matrix elements, $\left|W^{\mathrm{ie}}\right|^2 = |\langle \psi_{E'} | \boldsymbol{r}\cdot\boldsymbol{E} | \psi_0 \rangle|^2$ is the time-dependent excitation probability, which can be written as the population $\left|W^{\mathrm{ie}}\right|^2 \sim P_{E'} = |\langle \psi_{E'} | \psi(t) \rangle|^2$, W^{ic} is the photo-ionization probability of the intermediate resonant electronic state, which can be written as $\left|W^{\mathrm{ic}}\right|^2 = |\langle \psi_{\mathrm{c}} | \boldsymbol{r}\cdot\boldsymbol{E} | \psi_{E'} \rangle|^2 = \left|\sigma^{(1)}\mathcal{F}(\boldsymbol{E})\right|^2$, and $\sigma^{(1)}$ is the ionization amplitude. Obviously, the ionization probability W^{re} in Eq. (14) is sensitive to the population in the intermediate resonant state. Therefore, the induced magnetic field is closely related to the resonant excitation probability, which plays an essential role at $\lambda_0 = 70$ nm. This is also the main reason for the difference between the results at $\lambda_0 = 70$ nm and those at $\lambda_0 = 50$ nm.

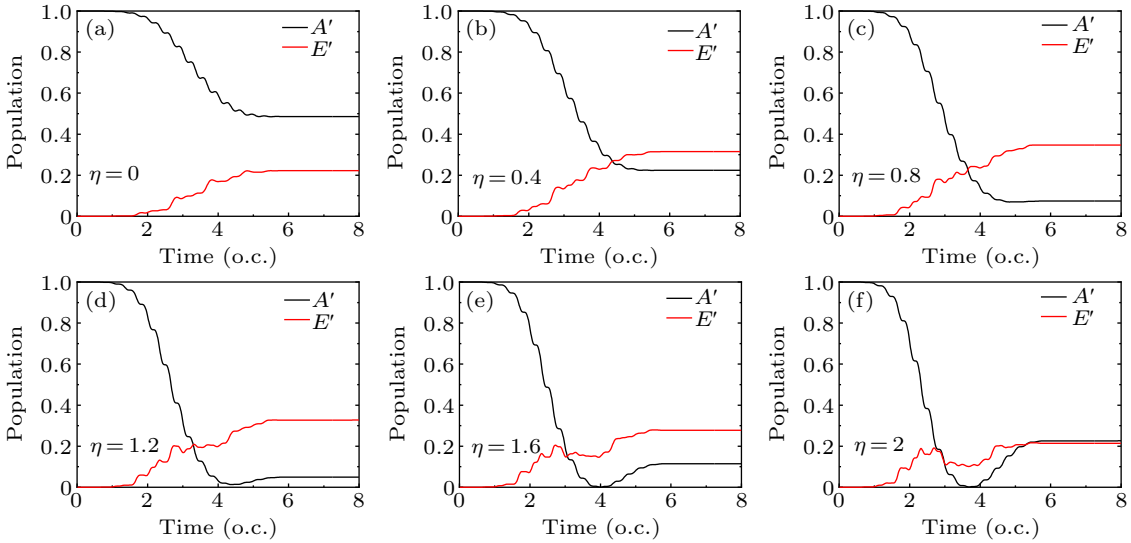


Fig. 5. Time-dependent probabilities $P(t)$ of the ground A' state (black line) and the excited E' state (red line) of H_3^{2+} under tricircular laser pulses with $\lambda_0 = 70$ nm of different η. The pulse intensity is $I_0 = 1\times10^{14}$ W/cm^2 and the duration is 6τ (cycles).

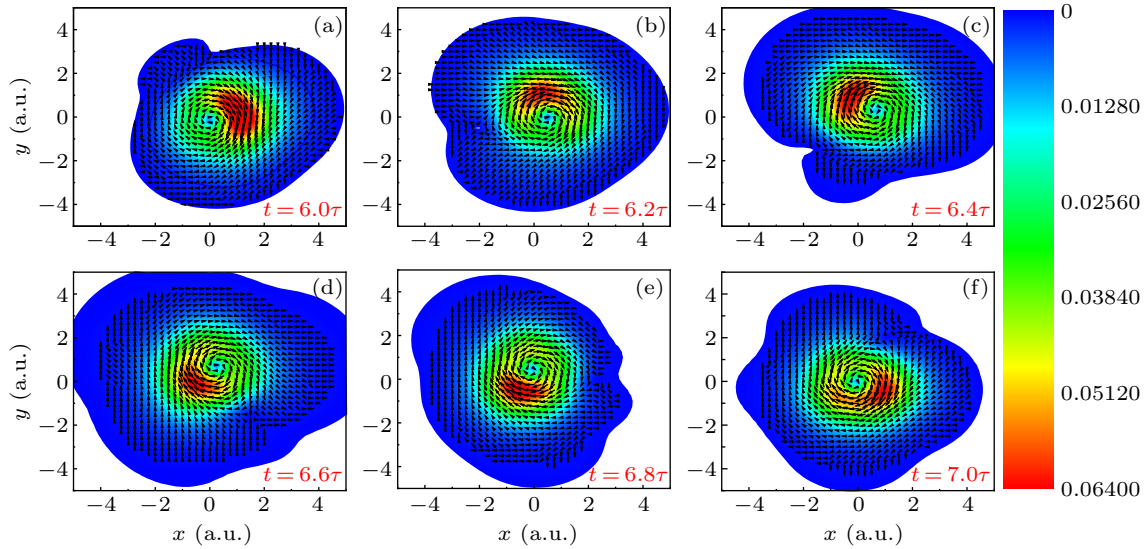


Fig. 6. Evolution of the electronic current distribution for different times t induced by a tricircular pulse with $\eta = 0.8$ and intensity $I_0 = 1\times10^{14}$ W/cm^2 ($E_0 = 0.0534$ a.u.) with $\lambda_1 = 70$ nm ($\omega_1 = 0.65$ a.u.), $\lambda_2 = 35$ nm ($\omega_2 = 1.30$ a.u.), $\lambda_3 = 17.5$ nm ($\omega_3 = 2.60$ a.u.), $\phi_{\omega_1} = \phi_{\omega_2} = \phi_{\omega_3} = 0$.

In order to support the above conclusion and explore the process of resonant excitation, we further compared the evolution of the population for ground and excited states with time. Figure 5 presents the population as a function of the time in the two electronic states $P_{\mathrm{gr}}(t) = |\langle \psi_{A'} | \psi(\boldsymbol{r},t) \rangle|^2$ for the ground A' state and $P_{\mathrm{ex}}(t) = |\langle \psi_{E'} | \psi(\boldsymbol{r},t) \rangle|^2 \sim \left|W^{\mathrm{ie}}\right|^2$ for the excited E' state at $\lambda_0 = 70$ nm with different η. As η increases from 0 to 0.8, the population of the ground state decreases, while that of the excited state increases, leading to an enhanced magnetic field. However, when η continues to increase, the population

transfers back to the ground state due to Rabi oscillations.[33] At this point, the population of the excited state decreases, so the magnetic field gradually weakens. This explains why the $\boldsymbol{B}_{\rm m}$ shown in Fig. 4(b) first increases when η increases from 0 to 0.8, then, as η continues to increase, $\boldsymbol{B}_{\rm m}$ is weakened. Meanwhile, we also calculated the ionization probability at $\lambda_0 = 50$ nm (see Fig. S1 in part 2 of the SI). It can be seen that the ionization probability increases with η, which is consistent with the change law of $\boldsymbol{B}_{\rm m}$ with η. Based on the above, it is known that changing η of the tricircular field can control magnetic field generation. Of course, here we also need to consider the effect of wavelength. The magnetic field obtained by the resonance mechanism is stronger, but it should be noted that for this mechanism a large η will suppress the excitation probability, thereby weakening the magnetic field.

In addition, coherent electron currents in charge transfer induced by a coherent superposition from resonant excitation are of great significance in photoinduced processes. We further study the distribution of electron currents at different times from $t = 6.0\tau$–7.0τ without an external electric field (Fig. 6). It can be clearly seen that under resonant excitation of A'–E' states, although the laser pulse is turned off, the electronic ring current evolves with a clockwise direction at different moments of 6.0τ–7.0τ. This result is consistent with a previous study,[16] and also confirms that the electrons circulate stably in the molecular rings.

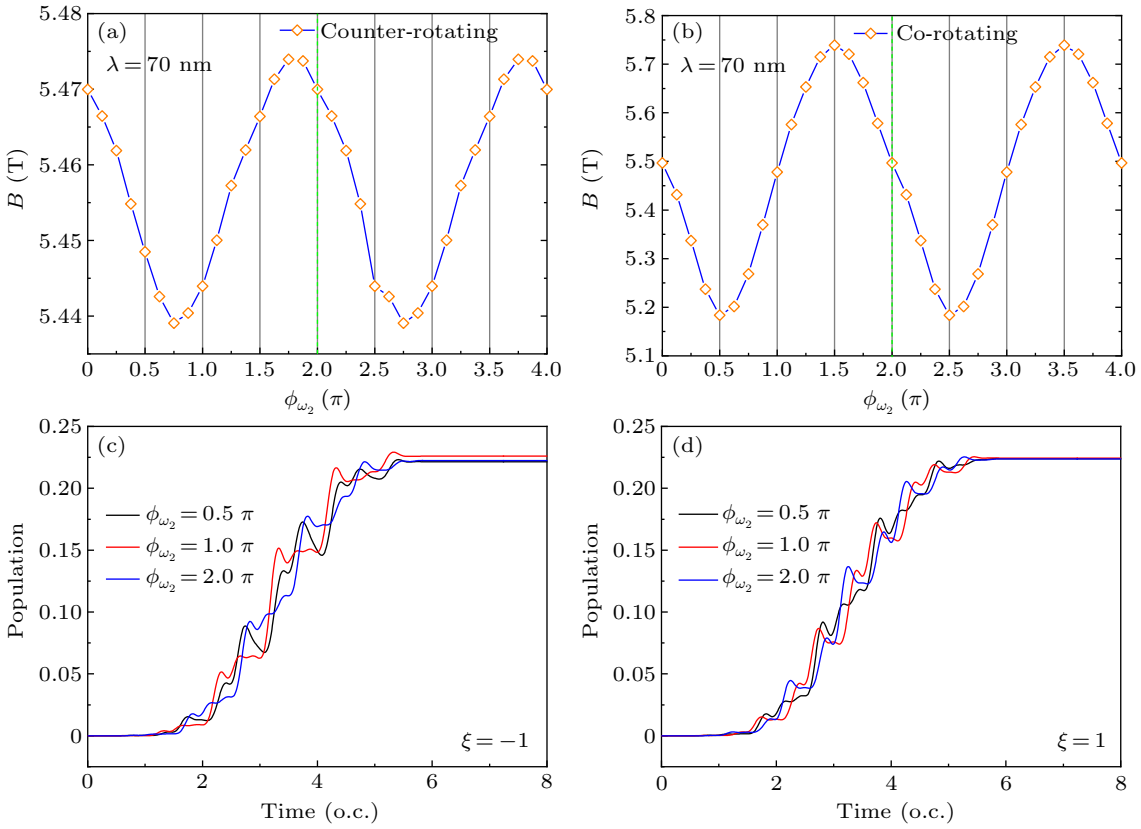


Fig. 7. Maximum values of the magnetic fields $\boldsymbol{B}(\boldsymbol{r} = 0, t)$ induced by (a) counter-rotating ($\xi_1 = -1$) and (b) co-rotating ($\xi_1 = +1$) bicircular laser pulses ($\omega_1 + \omega_2$, $\xi_1 = \pm 1$, $\eta = 0$) in Eq. (3). (c) and (d) Transition excitation probabilities from the ground A' state to the first excited E' state of H_3^{2+} ($\xi_1 = \pm 1$) with different CEPs ϕ_{ω_2}. The laser wavelengths are $\lambda_1 = 70$ nm ($\omega_1 = 0.65$ a.u.) and $\lambda_2 = 35$ nm ($\omega_2 = 1.30$ a.u.), the duration is 6τ (cycles) and the intensity is $I_0 = 1 \times 10^{14}$ W/cm^2.

In Eq. (3), if $\eta = 0$, the tricircular laser pulses are reduced to bicircular ones ($\omega_1 + \omega_2$, $\xi_1 = \pm 1$, $\eta = 0$, where $\xi_1 = -1$ represents the counter-rotating field and $\xi_1 = +1$ is the co-rotating field). We choose laser wavelengths of $\lambda_1 = 70$ nm and $\lambda_2 = 35$ nm to explore the effect of helicity and CEP on the magnetic field induced by bicircular pulses. Here, we fix $\phi_{\omega_1} = 0$ in the $\boldsymbol{E}_1(t)$ pulse and vary ϕ_{ω_2} in the $\boldsymbol{E}_2(t)$ pulse. Figures 7(a) and 7(b) show the maximum values of the induced magnetic field $\boldsymbol{B}(\boldsymbol{r} = 0, t)$. It was found that as CEP ϕ_{ω_2} varies from 0 to 4π in the counter- and co-rotating fields, the magnetic fields of both cases vary as a cos function of ϕ_{ω_2} and oscillate with a period of 2π. This result indicates that the generated magnetic field is sensitive to ϕ_{ω_2}, which can be attributed to the interference effect between multiple ionization pathways during the process of photoionization by the bicircular laser pulses. Specifically, for bicircular laser pulses with a wavelength of $\lambda_1 = 70$ nm or $\lambda_2 = 35$ nm, an electron needs to absorb three ω_1 photons or two ω_2 photons to ionize. According to the ultrafast ionization model, the total transition probability can be understood as the square of the two ampli-

tudes of the $\lambda_1 = 70$ nm and $\lambda_2 = 35$ nm laser pulses with an interference term of the two amplitudes (for more details see part 3 of the SI). The interference term can be written as

$$\begin{aligned} W^{(1,2)} &= W^{(1)*}W^{(2)} + W^{(1)}W^{(2)*} \\ &= 2\sigma^{(1)}\sigma^{(2)}E_0(\omega_1)^3 E_0(\omega_2)^2 \cos(\Delta\phi), \end{aligned} \quad (15)$$

where the relative phase is $\Delta\phi = 2\phi_{\omega_2} - 3\phi_{\omega_1}$ and $\phi_{\omega_1} = 0$. Therefore, according to Eq. (7), $\boldsymbol{B} \sim \cos(\Delta\phi)$. From this, we know that the relationship between the magnetic field and ϕ_{ω_2} should show a cos-like function curve, which explains the time-dependent magnetic field generation in Figs. 7(a) and 7(b). Furthermore, in order to ensure that it is caused by the interference term in the multiphoton ionization process rather than resonance, we also give the transition excitation probabilities from A'–E' at different ϕ_{ω_2} (Figs. 7(c) and 7(d)). The transition excitation probabilities are almost the same, which proves that the resonance excitation is not the reason why the dominant magnetic field is sensitive to the phase. Actually, for resonance excitation, the excited state transition probability is determined by the intrinsic transition dipole of molecules and the electric field strength and is insensitive to the pulse phase.[23]

4. Conclusion

In summary, we present a theoretical scheme to control the ultra-fast magnetic field generation of H_3^{2+} molecules induced by multi-frequency tricircular pulses composed of co- and counter-rotating circularly polarized laser pulses. The results show that the magnetic field strength is sensitive to the field amplitude (η) and the wavelength in the tricircular fields. Specifically, the strength of the magnetic field is linearly correlated with η at $\lambda_0 = 50$ nm under the multiphoton ionization mechanism. At $\lambda_0 = 70$ nm under resonance excitation the strength first increases and then decreases with increasing η. The main reason for this is that the transition excitation probabilities from the ground state to the first excited state are suppressed at larger η, resulting in a weaker magnetic field. Meanwhile, the electronic ring currents still exist even after the laser pulse is switched off at the resonance mechanism. Moreover, we also explore the effect of pulse phase and helicity on the magnetic field under bicircular pulses. It was found that the dependence of the generated magnetic field on the pulse phase arises from interference between multiple ionization pathways.

Acknowledgment

Project supported by the National Natural Science Foundation of China (Grant No. 12074146).

References

[1] Krausz F and Ivanov M 2009 *Rev. Mod. Phys.* **81** 163
[2] Chang Z G, Corkum P B and Leone S R 2016 *J. Opt. Soc. Am. B* **33** 1081
[3] Gaumnitz T, Jain A, Pertot Y, Huppert M, Jordan I, Ardana-Lamas F and Wörner H J 2017 *Opt. Express* **25** 27506
[4] Chelkowski S, Yudin G L and Bandrauk A D 2006 *J. Phys. B: At. Mol. Opt. Phys.* **39** S409
[5] Yuan K J, Chelkowski S and Bandrauk A D 2016 *Phys. Rev. A* **93** 053425
[6] Tan J, Zhou Y M, He M G, Chen Y B, Ke Q H, Liang J T, Zhu X S, Li M and Lu P X 2018 *Phys. Rev. Lett.* **121** 253203
[7] Vrakking M J J 2014 *Phys. Chem. Chem. Phys.* **16** 2775
[8] Kraus P M, Mignolet B, Baykusheva D, *et al.* 2015 *Science* **350** 790
[9] Böwering N, Lischke T, Schmidtke B, Müller N, Khalil T and Heinzmann U 2001 *Phys. Rev. Lett.* **86** 1187
[10] Xia C L and Miao X Y 2015 *Chin. Phys. Lett* **32** 043202
[11] Zhang H D, Guo J, Shi Y, Hui D, Liu H F, Huang X R, Liu X S and Jing J 2017 *Chin. Phys. Lett* **34** 014206
[12] Tsiatmas A, Atmatzakis E, Papasimakis N, *et al.* 2013 *New J. Phys.* **15** 113035
[13] Barth I, Manz J,Shigeta Y and Yagi K 2006 *J. Am. Chem. Soc.* **128** 7043
[14] Barth I and Manz J 2007 *Phys. Rev. A* **75** 012510
[15] Barth I , Manz J and L Serrano-Andrés L 2008 *Chem. Phys.* **347** 263
[16] Nobusada K and Yabana K 2007 *Phys. Rev. A* **75** 032518
[17] Lumb S, Talwar S L and Prasad V 2020 *J. Phys. B: At. Mol. Opt. Phys.* **53** 205002
[18] Yuan K J and Bandrauk A D 2013 *Phys. Rev. A* **88** 013417
[19] Yuan K J and Bandrauk A D 2015 *Phys. Rev. A* **91** 042509
[20] Yuan K J and Bandrauk A D 2015 *Phys. Rev. A* **92** 063401
[21] Bandrauk A D, Guo J and Yuan K J 2017 *J. Opt.* **19** 124016
[22] Xu Q Y, Yang Z J, He Y L, Gao F Y, Lu H Z and Guo J 2021 *Opt. Express* **29** 32312
[23] Bandrauk A D, Chelkowski S and Yuan K J 2021 *Front. Phys.* **9** 675375
[24] Guo J, Yuan K J, Lu H Z and Bandrauk A D 2019 *Phys. Rev. A* **99** 053416
[25] Yuan K J, Guo J and Bandrauk A D 2018 *Phys. Rev. A* **98** 043410
[26] Yang Z J, Xu Q Y, He Y L, Liu X S and Guo J 2021 *Chin. Phys. B* **30** 123203
[27] Jana K, Okocha E, Møller S H , Mi Y, Sederberg S and Corkum P B 2022 *Nano photonics* **11** 787
[28] Neufeld O and Cohen O 2018 *Phys. Rev. Lett.* **120** 133206
[29] Yuan K J and Bandrauk A D 2020 *Phys. Chem. Chem. Phys.* **22** 325
[30] Feit M D and Fleck Jr J A 1983 *J. Chem. Phys.* **78** 301
[31] Chu T S, Zhang Y, Han K L 2006 *Int. Rev. Phys. Chem.* **25** 201
[32] Jefimenko O D 1989 *Electricity and Magnetism: An Introduction to the Theory of Electric and Magnetic Fields* (Waynesburg: Electret Scientific)
[33] Bandrauk A D and Yuan K J 2016 *Mol. Phys.* **114** 344
[34] Pronin E A, Starace A F, Frolov M V and Manakov N L 2009 *Phys. Rev. A* **80** 063403
[35] Pronin E A, Starace A F and Peng L Y 2011 *Phys. Rev. A* **84** 013417
[36] Agostini P and Bensoussan P 1974 *Appl. Phys. Lett.* **24** 216